Development and Characterization of Novel Hybrid Materials Formed from ZnO-SiO2-Modified and Polyaniline for Organic Dyes Adsorption and Electrochemical Supercapacitor Applications

Imen Benchikh
Universite Amar Telidji Laghouat
Saadia Lahreche
Universite Dr Tahar Moulay de Saida
Youcef Benmimoun
Université de Mascara: Universite de Mascara
Abdelghani Benyoucef (a.benyoucel@univ-mascara.dz)
University of Mascara: Universite de Mascara https://orcid.org/0000-0002-0247-2808

Research Article

Keywords: Zinc oxide, Sol gel, Polyaniline, Adsorption, Supercapacitor.

Posted Date: March 31st, 2022

DOI: https://doi.org/10.21203/rs.3.rs-1479466/v1

Abstract

Polyaniline (PANI) coated ZnO-SiO_2 based hybrid material was prepared successfully by in-situ polymerization method and the product was analyzed by XPS, XRD, TEM, UV-vis, TGA, FTIR and BET techniques. According to these characterization results, ZnO were successfully incorporated with SiO_2 and PANI matrix was also supported on ZnO–SiO_2. The optical band gap was calculated from the Tauc's plot it has been found 2.89 eV. The development of a PANI@ZnO–SiO_2 is a new way to achieve better adsorption efficacy for Congo Red (CR) and Methylene Blue (MB) dyes in aqueous solutions due to the engineered excellent porous structure, which was 83.82 and 71.19 $mg.g^{-1}$, respectively. Moreover, this work reports also an extensive study of the effect of the SiO_2 on the electrochemical performance of hybrid material based on ZnO and PANI employing cyclic voltammetry. It was found that the perfect stability, which can be sustained during a longtime of the galvanostatic charge-discharge (GCD) operation. The results reveal a superior cycling stability, with 90.1% capacitance retention after 1500 cycles.

1. Introduction

In previous years, hybrid nanocomposite devices have received great attention owing to their outstanding electrical, optoelectronic, magnetic and adsorption properties, which open a large potential in applications as photovoltaic cells, supercapacitor, light emitting diodes, photodetectors, sensors, adsorption and transistors [1–8]. Hybrid materials have been widely explored due to their easy elaboration, low-cost production process, flexibilities, excellent reproducibility and versatile functionalities [9, 10 In nanocomposite devices nanoparticles NPs plays a crucial role in amelioration the electrical and optical properties of the devices. Presently, many investigations have been conducted to study the effect of NPs incorporation into conducting polymer backbone on the electron transfer process, such as charge trapping and detrapping [11, 12], the formation of conductive pathways [13] and the charge transfer between the organic products and NPs [14]. Moreover, the Polyaniline (PANI), a recognized promising conducting polymer, has attracted more and more attentions for the π-π conjugated electronic system, high absorption coefficients under visible light, high charge migration and good environmental stability [15, 16]. In addition, PANI attached to the surface of the NPs prevents self-aggregation, due to high surface energy [17]. Among the actually available inorganics, Zinc oxide (ZnO) is regarded as an important metal oxide, featuring advantages in terms of environmental sustainability, costs, as well as wide range absorption [18, 19]. Furthermore, the SiO_2 based products possess larger of porous, high specific surface area, tunable pore sizes, stable and interconnected structures [20, 21]. Herein, we demonstrated a facile and efficient method to synthesize multifunctional ZnO-SiO_2 structured as an advanced composite material. Unlike traditional process of obtaining nanocomposites by complicated multistep manufacturing procedure, the one step technique applied in this work is easy and effectual. For the first time, the application of PANI@ZnO-SiO_2 as adsorbents and as supercapacitors had been investigated. The major purpose of the current work was to synthesize and characterize these hybrid materials. The BET, XPS, XRD, FTIR, TGA, TEM, UV-vis and electrochemical behaviour methods were used to study the chemical microstructure and composition of samples.

2. Experimental

2.1. Materials

The deionized water used was purified through a Elga Labwater Purelab System. The chemicals including zinc oxide (ZnO, 95%), Ammoniumpersulfate (APS, ≥ 98%), Aniline (ANI, ≥ 99.5%), Tetraethyl orthosilicate (TEOS,

$C_8H_{20}O_4Si$, 98%), Ammonia solution (NH_4OH, 25%), Congo Red (CR) ($C_{32}H_{22}N_6Na_2O_6S_2$, ≥ 35%), Methylene Blue (MB) ($C_{16}H_{18}ClN_3S$), Hydrochloric acid (HCl, 70%), Nitric acid (HNO_3, 70%) and Tetrahydrofuran (THF) $(CH_2)_3CH_2O$, ≥ 99.9%) were purchased from Sigma-Aldrich. The Potassium hydroxide (KOH, 37%) and Ethanol (C_2H_5OH, 95%) were obtained from Merck.

2.2. Measurements

A H7500-Hitachi (Tokyo, Japan) transmission electron microscopy (TEM) was applied to examine the microstructure. A Bruker CCD-Apex (Madison-WI. USA) X−ray powder diffraction (XRD) with a CuK_α target was used to determine the main crystallinity parameters. The thermal stabilization of the samples structure was examined by Using a Thermogravimetric analysis (TGA) apparatus Hitachi STA7200 (Tokyo, Japan). The optical characteristics were determined using a Hitachi-U3000 spectrophotometer (Japan). Fourier transform infrared (FT-IR) spectroscopic were recorded between 500−4000 cm^{-1} (Bruker Instruments, Karlsruhe, Germany). The elemental composition and phase structures were determined by X-ray photoelectron spectroscopy (XPS) (3000electron, AVG-Microtech-Multilab; London, UK). The surface area of the materials was calculated using the Brunauer−Emmett−Teller (BET) technique using N_2 adsorption and desorption isotherms at 77K using an Autosorb-iQ instrument. Electrical conductivity measurement was carried out using 4-point probes method by Lucas Lab probe. The samples were dried at 70°C for overnight, and then pastilles have been prepared by a FTIR mold [18, 19, 22].

2.3. Fabricating ZnO-SiO_2

The ZnO-SiO_2 core shell nanoparticles were prepared by sol-gel method [23]. Briefly, 1.0 g ZnO and mixture solution containing 80 ml C_2H_5OH and 20 ml deionized H_2O were dispersed in an ultrasonic bath for 1h. Then, ammonia solution (0.5 mL) and 20 mL TEOS were added dropwise. The mixture was stirred for 24 h, centrifuged and washed with H_2O. The resulting composite was dried in a vacuum oven in order to get the ZnO embedded with the SiO_2.

2.4. Synthesis of PANI@ZnO-SiO_2

1.20 g ZnO-SiO_2 and 0.56 g of ANI were dispersed in ultrasonic for quarter hour, then 0.265 mL of HCl was dissolved in 160 mL H_2O and added to the mixture. This solution stirred for half hour at room temperature. Then 0.56 of APS which was stirred with 30 mL of H_2O added to it. The mixture was then stirred for another 24 h under magnetic stirring. Finally, the PANI@ZnO-SiO_2 obtained during the centrifugation process was washed several times with H_2O and C_2H_5OH, and placed in a dryer at 70° C for all night long [18, 24]. A graphical exemplification of the materials formation is presented in Scheme 1.

2.5. Electrochemical studies

The electrochemical characteristics of the samples were studied by cyclic voltammetry (CV) using a conventional 3-electrodes electrochemical system [22, 25].

3. Results And Discussion

3.1. Structural and morphological analysis

The FTIR spectra of ZnO, ZnO−SiO_2, PANI and PANI@ZnO−SiO_2 are shown in Fig. 1-a. The strong stretching mode of the O−Zn−O bond is observed in the range spanning from 540 cm^{-1} to 555 cm^{-1} for all the samples, while the

wide band in ZnO spectrum at approximately 3446 cm^{-1} is attributed to the –OH groups of water, indicating the presence of H_2O absorbed on the ZnO surface. Moreover, a new band appears at 1058 cm^{-1} in the ZnO–SiO_2 composite, associated to the asymmetric and symmetric stretching vibrations of Si–O–Si. Another new absorption at 951 cm^{-1} indicates the existence of perturbing or defect groups, and could be correspond to asymmetric stretching of Si–O bond neighboring surface silanol groups [29]. On the other hand, the IR spectrums of PANI show the principal characteristic peaks of the samples at 1592 cm^{-1}, 1497 cm^{-1}, 1376 cm^{-1}, 1309 cm^{-1}, 1164 cm^{-1} and 825 cm^{-1} in agreement with the literature [30]. The spectrum exhibits two bands at 1592 cm^{-1} and 1497 cm^{-1} are to the stretchin vibrations of the quinoid/benzenoid (Q/B) units of polyaniline [18, 22]. The band at 1376 cm^{-1} is to the C, N^+ stretching adjacent to the Q structure while that a band near 1309 cm^{-1} is ascribed to C–N stretching vibration in the alternate rings of Q–B–Q units. The two bands at 1376 cm^{-1} and 1309 cm^{-1} attributed to N–H bending and the symmetric component of the C–C (or C–N) stretching modes. The absorption band at 1164 cm^{-1} is a characteristic of the electronic-like absorption of the N = Q = N vibration (where Q denotes out-of-plane bending vibration of the para-substituted benzene unit). Finally, the band at 3283 cm^{-1} is corresponding to N–H stretching frequency. For PANI@ZnO–SiO_2, the PANI characteristic bands around 1560 cm^{-1}, 1491 cm^{-1}, 1441 cm^{-1}, 1284 cm^{-1}, 1161 cm^{-1} and 825 cm^{-1} were retained. Besides, the Si–O–Si characteristic bound at 1060 cm^{-1} appeared, indicating that ZnO–SiO_2 composite was successfully loaded and combined with PANI matrix.

Figure 1-b. depicts a XPS survey scan spectra of the bonding states and chemical structural of materials synthesized. Generally, the main elements are C, O, N, Zn, Si and suggest that there are no impurities in the samples. Figure 2-a. presents the highresolution Zn2p XPS spectrum of the ZnO sample with two bands at 1045 and 1022 eV, corresponding to Zn2p1/2 and Zn2p3/2, respectively. In addition to these two peaks, a new peak appeared for ZnO–SiO_2 composite corresponding to Si2p, and the deconvolution of this peak yielded a peak at 103.62 eV and 104.58 eV which are corresponding to Si2p3/2 and Si2p1/2, respectively (Fig. 3-a). Likewise, the high-resolution spectra for Zn2p and Si2p provide details of the bonding information of PANI@ZnO–SiO_2 (Table 1). Meanwhile, the O1s of ZnO has two peaks appeared at 531.81 eV and 533.62 eV respectively (Fig. 3-b), corresponding to O–H and O–Zn, which was consistent with the conclusion of FTIR analysis. In addition, these two binding energies shifted to 531.41 eV and 533.42 eV, with the appearance of a new third peak at 532.39 eV assigned to O–Si, these changes indicated that the ZnO–SiO_2 composite was successfully produced. To better understand the role of ZnO–SiO_2 in the PANI matrix, XPS spectra values of the hybrid material are shown in Table 1. Hence, it can be concluded that O–H, O–Si and O–Zn existed in the PANI@ZnO–SiO_2.

Table 1
Summary of the XPS binding energy values (eV) obtained for hybrid materials.

Binding Energy / eV	ZnO	ZnO-SiO_2	PANI	PANI@ZnO-SiO_2	Assignments
O1s	531.81	531.41	//	531.77	O-H
	//	532.39	//	532.56	O-Si
	533.62	533.42	//	533.51	O-Zn
N1s	//	//	398.97	398.35	–N=
	//	//	400.36	400.42	$-NH_2$; –NH–
	//	//	401.55	401.47	$-NH^+$
Si2p	//	103.62	//	103.62	Si–O
	//	104.58	//	104.58	Si-O_2
Zn2p	1022	1025	//	1026	Zn2p3/2
	1045	1047	//	1049	Zn2p1/2

The N1s spectrum of PANI had three peaks located at 398.97 eV, 400.36 eV and 401.55 eV (Fig. 3-c), which corresponded to the (–N=), ($-NH_2$ or –NH–) and ($-NH^+$), respectively [24]. For PANI@ZnO–SiO_2, the binding energies of the characteristic peaks of N1s shifted respectively to 398.35 eV, 400.42 eV and 401.47 eV. Additionally, the N1s spectrum of PANI contains three kinds electronic states of the quinoid imine (= N–) at 398.97 eV, benzenoid amine ($-NH_2$) at 400.36 eV and the cationic radical ($-NH^+$) at 401.55 eV (Fig. 3-d) [26, 27]. Moreover, the N1s core-level spectrum of PANI@ZnO–SiO_2 (Fig. 4-b) presented also three main peaks at 398.35 eV, 400.42 eV and 401.47 eV, which were attributed to (= N–), (–NH–) and ($-NH^+$), respectively. Furthermore, the oxidation degree and protonation of PANI chain can be measured by analyzing the ratios of (–N=), (–NH–) and ($-NH^+$) [18, 22]. The PANI matrix in hybrid materials contained 1.64% (= N–) and 0.85% (–NH–). The ratio of (–N=) to (–NH–) was about 1.93 for pure PANI, whereas that hybrid material contained 1.24% (= N–) and 0.87% (–NH–), with the ratio of (= N–/–NH–) higher to 0.01. Especially, the total of ($-NH^+$) in the PANI@ZnO–SiO_2 is higher compared to pure PANI, resulting a comparatively higher doping level (DL) of PANI matrix into PANI@ZnO–SiO_2 (Table 2). The increased ratio of $-NH^+$ could be due to the interactions between PANI matrix with ZnO–SiO_2 composite that links to the restructuring of the ($-NH_2$) group in the PANI backbone [28]. Further, the high (DL) is expected to ameliorate its pseudocapacitive performance as electrodes, and also that probable results in its more rapidly charge-discharge rate and considerable capacitance [22].

Table 2
The atomic percentage (%) and Redox peak of hybrid materials synthesized.

Materials	C1s	N1s	O1s	Si2p	Zn2p	DL*	FD**	$E_{ox1/red1}$	ΔE_{p1}	$E_{ox2/red2}$	ΔE_{p2}
PANI	83.19	11.02	5.79	//	//	0.50	0.41	0,45/0.29	0.16	0.89/0,81	0.08
PANI@ZnO-SiO_2	78.82	9.14	1.98	4.74	5.32	0.62	0.27	0,50/0.30	0.20	0,89/0.75	0.10

$(DL^{*})\ DopingLevel = \frac{high binding energy band}{total band area}$; $(FD^{**}) Flaws Density = \frac{lowest binding energy band of N1s}{total band area of N1s}$

Figure 4-a. displays the XRD patterns of samples. The prominent Bragg reflections planes of structure ZnO were observed at 2θ values around 31.77º, 34.39º, 36.23º, 47.52º, 56.56º, 62.83º, 67.93º and 69.09º, which are assigned to the (100), (002), (101), (102), (110), (103), (112) and (201) crystallographic planes respectively, which corroborates with the JCPDS 36–1451 card number well. For the ZnO–SiO_2 composite along with all intense peaks of ZnO, another broad peak was observed at 24.17º. Thereby, the diffraction pattern of the as-prepared materials display the combinational peak signals of both ZnO (JCPDS 36–1451) and SiO_2 (JCPDS 29–0085), showing that it are crystal morphology and verifying the successful formation of the nanocomposite structure. Furthermore, PANI is semi-crystalline in character as the patterns illustrate three clear peaks at 2θ = 9.16º (011), 20.98° (020) and 26.24° (200) due to existence of Q with B rings in the PANI backbone [29]. Besides, it is evident that the feature absorption peaks of ZnO–SiO_2 composite are reserved in hybrid material. Moreover, a further weak peak between 20°–30º was appertaining to the feature absorption peak of polymer chain [30], shows in the formed core-shell-structure PANI@ZnO–SiO_2 by comparing them with the graphs of neat ZnO–SiO_2. These results confirm that the hybrid materials have been successfully prepared by in–situ polymerization technology.

The specific surface area and pore size distribution of ZnO, ZnO–SiO_2, PANI and PANI@ZnO–SiO_2 were measured using N_2 adsorption-desorption isotherms (Fig. 4-b and Table 3). Referring to the IUPAC classification, the adsorption and desorption isotherms should be type IV, which indicated that they have a mesoporous structure [31]. According to the pore size distribution, there were abundant micropores and mesopores in ZnO–SiO_2 and PANI@ZnO–SiO_2, which is beneficial to the transport and stabilization of pollutants. After ZnO–SiO_2 modification, the BET surface area decreased from 196 $m^2. g^{-1}$ to 108 $m^2. g^{-1}$. The loading of PANI matrix blocked the pores of inorganic composite. However, the total pore volume and pore size of PANI@ZnO–SiO_2 are larger than pure PANI, which provide additional binding sites for pollutants. Similar phenomena have been obtained in other studies [21, 32].

Table 3
Textural characterization and Surface composition (at%) from XPS of adsorbents prepared before and after adsorption.

Materials	PANI	ZnO	ZnO-SiO_2	PANI@ZnO-SiO_2
S_{BET} / $m^2.g^{-1}$	27	4	196	108
V_{DR} (N_2) / $cm^3.g^{-1}$	1.11	0.92	1.37	1.24
V_{mes} / $cm^3.g^{-1}$	0.01	0.01	0.09	0.08
V_{mic} / $cm^3.g^{-1}$	0.01	0.02	0.15	0.13
V_{tot} pore	0.02	0.03	0.24	0.21

Table 4
The adsorptive capacity of several adsorbents for removal of CR and MB dyes.

Dyes	Adsorbents	Adsorption Efficiency	Ref.
CR	PANI@ZnO	69.82	[18]
	PVC@graphene-polyaniline	14.94	[33]
	Polyaniline	50	[34]
	PANI@SiO_2	71	[35]
	Pani@MoS_2	70.92	[36]
	PANI/ZTO	64.51	[37]
	Chitosan/montmorillonite nanocomposite	54.52	[38]
	PANI@ZnO–SiO_2	83.82	This work
MB	PANI@ZnO	59.23	[18]
	PANI zirconium (IV) silicophosphate	8.8	[39]
	CDs initiated PANI	18	[40]
	CDs initiated PPY	16	[40]
	PANI/zirconium oxide	35	[41]
	Polyaniline nanotube base/silica composite)	5.38	[42]
	SW–ZnO–PANI hybrid composite	20.55	[43]
	Polyaniline nanotubes	9.21	[44]
	PANI@ZnO–SiO_2	71.19	This work

The thermal performances of samples were also evaluated by thermogravimetric analysis (TGA) in the temperature range of 25–900ºC as in Fig. 2-b. ZnO underwent a limited mass loss up to 110°C, attributed to desorption of water

and gases. On the contrary, ZnO–SiO_2 exhibited the main mass loss between ca 500 and 900°C, due to the degradation of the SiO_2 not interacting with the ZnO surface. For PANI@ZnO–SiO_2, the weight loss curve was obviously divided three decomposition regions. In the region of 25ºC and 180ºC, this weight loss was assigned to the evaporation of the moisture. The weight loss in the range of 220ºC and 450ºC was related to the degradation of the PANI chain. The weight loss in the region of 450ºC and 630ºC was attributed further degradation of the PANI molecular chains. Compared with PANI, the weight loss of polymer was mainly concentrated on the region of 340ºC and 610ºC, which was also related to the degradation of the PANI molecular chains [29]. Moreover, the initial weight loss between 25ºC and 190ºC was similarly attributed to the evaporation of the moisture. Over all, weight loss of ZnO–SiO_2 is 28.78% and of PANI@ZnO–SiO_2 is 66.15% in the temperature range from 25 to 900°C. Whereas, pure PANI exhibited an important weight loss of most than 85.92% till 900°C. Even though temperature changes effect of the products proprieties, the synthesis of hybrid materials based ZnO–SiO_2 improves this products efficiency compared to pure PANI, and this performance associated with the strength and durability of the bonding between the inorganic composites and PANI matrix.

The prepared materials were characterized by TEM. The result was exhibited in Fig. 5. It could be seen that that most of the resulting ZnO is almost spherical and dispersed on the supports (Fig. 5-a). Moreover, we find that ZnO–SiO_2 composite does not change the size of neat ZnO significantly and it is primarily uniform and few of them were slightly stuck together, as shown in Fig. 5-b. This TEM analysis confirmed that this composite were prepared successfully. Meanwhile, Fig. 5-c shows that the PANI@ZnO–SiO_2 show notable deformation and their surface became rough in the presence of PANI matrix. This TEM image confirms that the ZnO–SiO_2 composite is coated with a thin coat of polymer. This result proved ZnO–SiO_2 is connected by PANI coats.

Figure 6-a. displays the UV-Vis spectra of PANI and PANI@ZnO–SiO_2. Two absorption peaks at about 340–342 nm and 565–566 nm were observed. The first absorption band located is associated to the π–π* transition in the B unit [18, 19]. The second absorption band is assigned to the transition Q unit (charge transfer from HOMO of the B unit to LUMO of the Q unit) [25]. These bands provide information on the general oxidation state of PANI.

The gap energy (E_g) of the synthesized samples was determined from the UV-Vis spectrum. Figure 6-b. shows the variation of ($\alpha h\nu$) as a function of ($h\nu$) the gap energy (E_g) of nanoparticles is estimated using Tauc's formula [22]:

$$(ah\nu)^n = B(h\nu - E_g)$$

B

is a constant and represents the energy of the incident photon.

α: the absorption coefficient.

E_g

the optical bandgap in electron volts (eV).

n: is an variable exponent that depends on the nature of the electronic transition (when the transition is direct n = 2, and when transition is indirect n = ½) [22].

The optical energy band gap of the PANI and PANI@ZnO–SiO_2 are 3.21 eV and 2.89 eV, respectively. Thereby, the E_g value of hybrid material has reduced compared to neat PANI due to the strong interactions between ZnO–SiO_2 and PANI matrix, which caused changes in the electron density of the polymer backbone.

3.2. PANI@ZnO–SiO_2 Applications

3.2.1. Adsorption capacities for organic dyes

Dye as one of the main sources of pollution severely threatens human's health and the ecology of environment. In order to remediate our eco-environment system, it is urgent to develop the novel adsorbent with superior performance in removing the dyes. In this study, the dye adsorption performance of the as-synthesized PANI@ZnO–SiO_2 was evaluated. Two kinds of dyes, Congo Red (CR) and Methylene Blue (MB) were chosen as the aimed dyes. The procedures of dye adsorption experiments were described as follow: 50 mg adsorbent was filled into 100 mL CR and MB aqueous solution with the concentration of 100 $mg.L^{-1}$, respectively. The flasks were agitated at 150 rpm for 4 h. Finally, the mixture was filtered and prepared for UV–Vis spectrophotometer at 497 nm and 660 nm, respectively. The uptake of dye for hybrid material was calculated by the following equation:

$$Q_e = \frac{(C_0 - C_{eq})V}{m}$$

Where C_0 and C_e represent the initial and equilibrium concentrations of dye solution, respectively; V denotes the volume of the dye solution; and m represents the mass of adsorbent.

The results were displayed in Fig. 7-a. The adsorption capacities of CR and MB dyes were 83.82 $mg.g^{-1}$ and 71.19 $mg.g^{-1}$, respectively. These values were higher than many adsorbents to remove CR and MB dyes from the solution [18, 33–44]. Compared with those reported adsorbents, the resulting hybrid material displayed higher affinities with these two dyes. These results were probably attributed to their high apparent surface areas. That is, when the PANI@ZnO–SiO_2 was added to CR and MB, under the acidic condition, those $-NH_2^+-$, $-NH^+=$, –NH– and –N = on the PANI matrix could easily approach the groups of $-SO_3^-$, $-COO^-$and –NH– in dyes through electrostatic interaction and hydrogen interaction [35]. Thus, the dyes could be easily removed at relatively higher adsorption capacities.

3.2.2. Electrochemical Performance

To assure that the hybrid materials have a possibility of fabricating electrodes for supercapacitor, the electrochemical characterization were tested by cyclic voltammetry (CV), galvanostatic (GCD) and cyclic stability.

Since the CV of PANI has been reported widely in literature before, they are only briefly displayed here. Figure 7-b. presents the CVs of the samples over a potential between 0.0V to 1.0V, with a scan rate of 50$mV.s^{-1}$. The two samples offer an almost rectangular form and consist of a combination of double layer capacitor and pseudo capacitor with its two redox couples. The first redox couple (A/A') is attributed with the transition of the totally reduced Leucoemeraldine-base (LB) to the partly oxidized Emeraldine-salt (ES), and the second redox peaks (B/B') relates to the transition of (ES) to the entirely oxidized pernigraniline form (PB). These typical peaks are due to redox transformation of PANI, suggesting that the PANI-like character dominates in the PANI@ZnO–SiO_2. The presence of ZnO–SiO_2 composite in this hybrid material resulted in a shift of potential peak separation (ΔE_p) to

higher values compared to neat PANI (Table 2). This proves that the reaction kinetic is surface bounded and the electrochemical characteristics are changed also by the $ZnO–SiO_2$ composite formed on PANI matrix, indicating its strong interactions with polymer backbone. Such interactions results in highly porosity and rough surfaces, providing larger electrode-electrolyte interface area for more redox systems [19, 21].

The cycling behavior is one of the important critical indices in the practical employ of electrodes supercapacitors. The long-term stability of as-formed electrodes was tested by galvanostatic charge/discharge (GCD), and the results are offered in Fig. 8-a. The GCD which were executed the potential range from 0.0 to 0.8V and at a current density of 1.5 $A{\cdot}g^{-1}$. Generally, the GCD curves of these samples have an asymmetric distorted triangular shape with an evident plateau due to the faradaic character of the electrode prepared [22]. The charging slopes of $PANI@ZnO–SiO_2$ illustrated a rapid voltage rise from 0.0V to 0.15V, which was also because the equivalent-series-resistance (ESR), followed by a curve flattened at around 0.15V to 0.26V, due to the oxidation from ES to PB, the essential redox conversion where energy is stocked [45], pursued by a another flattening of the curve at about 0.40V to 0.45V. Then following ascent was then curve steep to 0.8V, then continuous decline for this curve. Accordingly, high GCD time observed in this case compared to neat PANI illustrates the high charge storage capacity of this hybrid material electrode. It can be clarified by the porous interconnected structural character of the PANI matrix and the synergy between ZnO and SiO_2. Thereby, it is evident that the existence of crystalline $ZnO–SiO_2$ composite with new porosity could reinforce the $PANI@ZnO–SiO_2$ stability [46]. This result also proved that this hybrid material had an excellent electrochemical reversibility.

Cycling stability (CS) is a critical factor for operational supercapacitor. Particularly, supercapacitor based on polymer frequently experience limited CS due to the shrinking and swelling of the polymer during its GCD process [47]. Figure 8-b. displays the samples' CS performance at the current density of 1.5 $A.g^{-1}$. It is found that capacitance retention of PANI is fading with growing number of cycles achieving 62.9% after 1500 cycles (Fig. 8-c) [48]. Furthermore, the capacitance retention of $PANI@ZnO–SiO_2$ (90.1%) is higher than that of neat PANI, showing the beneficial impact of $ZnO–SiO_2$ composite. In other words, the presence of this composite can play a key role in the enhancement of PANI chain electrochemical performances.

4. Conclusions

Hybrid material based ZnO and SiO_2 were successfully prepared to supported and enhance stabilization of the PANI matrix. The resultant products were analyzed by BET, XPS, FTIR, XRD, UV-vis, TEM and TGA. Furthermore, the optical bandgap was also tested. The development of a $PANI@ZnO–SiO_2$ is a new way to achieve good adsorption efficacy for Congo Red (CR) and Methylene Blue (MB) dyes in aqueous solutions due to the engineered high-performance open porous structure, which was 83.82 and 71.19 $mg.g^{-1}$, respectively. Moreover, the results of the electrochemical performance reveal that the $PANI@ZnO–SiO_2$ appear to have perfect stability, which can be sustained during a longtime of the GCD operation. As a result, $ZnO–SiO_2$ composite effectively improves the cycling stability of PANI backbone even at high discharge rates (90.1% after 1500 cycles).

Declarations

Acknowledgements:

The authors would like to express their gratitude to the Algerian DGRSDT-MESRS for their contributions to the scientific findings. The authors also would like to thank IUMA of Alicante University Spain researchers for their supports and co-operation availing.

Funding information:

There are no sources funding.

Conflict of Interest:

The authors declare that they have no conflict of interest

References

[1] C. Yoon, K. Yang, J. Kim, K. Shin, K. Lee. Fabrication of highly transparent and luminescent quantum dot/polymer nanocomposite for light emitting diode using amphiphilic polymer-modified quantum dots. Chemical Engineering Journal . 382 (2020) 122792

[2] A. Benchaabane, Z. Ben Hamed, A. Telfah, M.A. Sanhoury, F. Kouki, K. Zellama, H. Bouchriha. Effect of OA-ZnSe nanoparticles incorporation on the performance of PVK organic photovoltaic cells. Materials Science in Semiconductor Processing . 64 (2017) 115-123

[3] A.V. Kesavan, M.P. Kumar, A.D. Rao, P.C. Ramamurthy. Light management through up-conversion and scattering mechanism of rare earth nanoparticle in polymer photovoltaics. Optical Materials. 94 (2019) 286-293

[4] F. Ma, Q. Zhang, C.Y. Zhang. Catalytic Self-Assembly of Quantum-Dot-Based MicroRNA Nanosensor Directed by Toehold-Mediated Strand Displacement Cascade. Nano Letters. 19 (2019) 6370-6376

[5] L. Zhang, P. Wan, T. Xu, C. Kan, M. Jiang. Flexible ultraviolet photodetector based on single ZnOmicrowire/polyaniline heterojunctions. Optics Express. 29 (2021) 19202-19213

[6] S.S. Omprakash, S.K.N. Kumar. PANI/ZnO Hybrid Nanocomposites TFT for NAND Gate Application. Materials Today: Proceedings. 5 (2018) 10827-10832

[7] J.G. Kim, D.M. Lee, J.Y. Jung, M.J. Kim, M.S. Khil, H.S. Jeong, N.D. Kim. Hybrid Polyaniline/Liquid Crystalline CNT Fiber Composite for Ultimate Flexible Supercapacitors. ACS Applied Energy Materials. 4 (2021) 1130-1142

[8] S. Lahreche, I. Moulefera, A. El Kebir, L. Sabantina, M. Kaid, A. Benyoucef. Application of Activated Carbon Adsorbents Prepared from Prickly Pear Fruit Seeds and a Conductive Polymer Matrix to Remove Congo Red from Aqueous Solutions. Fibers.10 (2022) 7.

[9] A. Singh, A. Dey, P.K. Iyer. Collective effect of hybrid Au-Ag nanoparticles and organic-inorganic cathode interfacial layers for high performance polymer solar cell.Solar Energy. 173 (2018) 429-436

[10] E. Salima, S.R. Bobbarab, A. Orabya, J.M. Nunzi. Copper oxide nanoparticledopedbulk-heterojunctionphotovoltaicdevices. SyntheticMetals. 252 (2019) 21-28

[11] J.H. Son, D.H. Kim, W.K. Park, F. Li Choi, J.H. Ham, T.W. Kim. Nonvolatile flexible organic bistable devices fabricated utilizing CdSe/ZnS nanoparticles embedded in a conducting poly N-vinylcarbazole polymer layer.

Nanotechnology. 19 (2008) 055204

[12] W.L. Leong, P.S. Lee, S.G. Mhaisklkar, T.P. Chen, A. Dodablapur. Charging phenomena in pentacene- gold nanoparticle memory device.Applied Physics Letters. 90 (2007) 042906

[13] M. Vilkman, K. Solehmainen, A. Laiho, H.G.O. Sandberg, O. Ikkala. Negative differential resistance in polymeric memory devices containing disordered block copolymers with semiconducting block. Organic Electronics. 10 (2009) 1478-1482.

[14] E. Kolesova, V. Maslov, F. Safin, F.P. Milton, O. Cleary, Y. Volkov, Y.K. Gunko, A. Orlova. Photoinduced Charge Transfer in Hybrid Structures Based on Titanium Dioxide NPs with Multicomponent QD Exciton Luminescence Decay. Journal of Physical Chemistry C. 123 (2019) 14790-14796.

[15] L. Ge, C. Han, J. Liu. In situ synthesis and enhanced visible light photocatalytic activities of novel PANI–gC3N4 composite photocatalysts. Journal of Materials Chemistry. 22 (2012) 11843-11850

[16] M.O. Ansari, M.M. Khan, S.A. Ansari, J. Lee, M.H. Cho. Enhanced thermoelectric behaviour and visible light activity of Ag@TiO_2/polyaniline nanocomposite synthesized by biogenic-chemical route.RSC Advances. 4 (2014) 23713-23719

[17] X. Wang, D. Wu, X. Song, W. Du, X. Zhao, D. Zhang. Review on Carbon/Polyaniline Hybrids: Design and Synthesis for Supercapacitor. Molecules. 24 (2019) 2263

[18] I. Toumi, H. Djelad, F. Chouli, A. Benyoucef. Synthesis of PANI@ZnO Hybrid Material and Evaluations in Adsorption of Congo Red and Methylene Blue Dyes: Structural Characterization and Adsorption Performance. Journal of Inorganic and Organometallic Polymers and Materials. 32 (2022) 112-121

[19] S. Bousalem. F.Z. Zeggai. H. Baltach. A. Benyoucef. Physical and electrochemical investigations on hybrid materials synthesized by polyaniline with various amounts of ZnO nanoparticle.Chemical Physics Letters.741 (2020) 137095.

[20] F. Nador, E. Guisasola, A. Baeza, M. A. Villaecija, M.V. Regi, D.R. Molina. Synthesis of Polydopamine-Like Nanocapsules via Removal of a Sacrificial Mesoporous Silica Template with Water Chemistry-A European Journal. 23 (2017) 2753–2758.

[21] D. Huang, Y. Zhang, J. Zhang, H. Wang, M. Wang, C. Wu, D. Cheng, Y. Chi, Z. Zhao. The synergetic effect of a structure-engineered mesoporous SiO2–ZnO composite for doxycycline adsorption.RSC Advances.9 (2019) 38772.

[22] A. Bekhoukh, I. Moulefera, L. Sabantina, A. Benyoucef. Development, Investigation, and Comparative Study of the Effects of Various Metal Oxides on Optical Electrochemical Properties Using a Doped PANI Matrix.Polymers. 13 (2021) 3344.

[23] A. Benchaabane, M.E. Hajlaoui, N. Hnainia, A. Al-Tabbakh, A. Zeinert, H. Bouchriha. Optical properties enhancement of hybrid nanocomposites thin films based on P3HT matrix and ZnO@SiO_2 core-shell nanoparticles. Optical Materials.102 (2020) 109829.

[24] M. Zenasni, A.Q. Jaime, A. Benyoucef, A. Benghalem. Synthesis and characterization of polymer/V_2O_5 composites based on poly(2-aminodiphenylamine). Polymer Composites. 42 (2021) 1064-1074.

[25] I. Radja, H. Djelad, E. Morallon, A. Benyoucef. Characterization and electrochemical properties of conducting nanocomposites synthesized from p-anisidine and aniline with titanium carbide by chemical oxidative method. Synthetic Metals. 202 (2015) 25-32.

[26] Y. Li, Z. Xia, Q. Gong, X. Liu, Y. Yang, C. Chen, C. Qian. Green Synthesis of Free Standing Cellulose/Graphene Oxide/Polyaniline Aerogel Electrode for High-Performance Flexible All-Solid-State Supercapacitors.Nanomaterials.10 (2020) 1546.

[27] T. Lin, W. Liu, B. Yan, J. Li, Y. Lin, Y. Zhao, Z. Shi, S. Chen. Self-Assembled Polyaniline/Ti_3C_2Tx Nanocomposites for High-Performance Electrochromic Films.Nanomaterials.11 (2021) 2956.

[28] L. Yueqin, X. Zongbiao, G. Qiang, L. Xiaohui, Y. Yong, C. Chen, Q. Changhao. Green Synthesis of Free Standing Cellulose/Graphene Oxide/Polyaniline Aerogel Electrode for High-Performance Flexible All-Solid-State Supercapacitors.Nanomaterials.10 (2020) 1546.

[29] L. Maaza, F. Djafri, A. Belmokhtar, A. Benyoucef. Evaluation of the influence of Al_2O_3 nanoparticles on the thermal stability and optical and electrochemical properties of PANI-derived matrix reinforced conducting polymer composites. Journal of Physics and Chemistry of Solids.152 (2021) 109970.

[30] Y. You, Y. Wang, L. Tu, L. Tong, R. Wei, X. Liu. Interface Modulation of Core-Shell Structured $BaTiO_3$@polyaniline for Novel Dielectric Materials from Its Nanocomposite with Polyarylene Ether Nitrile. Polymers. 10 (2018) 1378.

[31] R. Girimonte, F. Testa, M. Turano, G. Leone, M. Gallo, G. Golemme. Amine-Functionalized Mesoporous Silica Adsorbent for CO_2 Capture in Confined-Fluidized Bed: Study of the Breakthrough Adsorption Curves as a Function of Several Operating Variables. Processes.10 (2022) 42.

[32] S. Daikh, D. Ouis, A. Benyoucef, B. Mouffok. Equilibrium, kinetic and thermodynamic studies for evaluation of adsorption capacity of a new potential hybrid adsorbent based on polyaniline and chitosan for Acetaminophen.Chemical Physics Letters.17 (2022) 139565.

[33] R. Kumar, M.O. Ansari, N. Parveen, M.A. Barakat, M.H. Cho. Simple route for the generation of differently functionalized PVC@graphene-polyaniline fiber bundles for the removal of Congo red from wastewater. RSC Advances. 5 (2015) 61486-61494.

[34] H. Chafai, M. Laabd, S. Elbariji, M. Bazzaoui, A. Albourine. Study of congo red adsorption on the polyaniline and polypyrrole. Journal of Dispersion Science and Technology. 38 (2017) 832-836.

[35] M. Maruthapandi, L. Eswaran, J.H.T. Luong, A. Gedanken. Sonochemical preparation of polyaniline@TiO2 and polyaniline@SiO_2 for the removal of anionic and cationic dyes.UltrasonicsSonochemistry.62 (2020) 104864.

[36] R. Kumar, S.A. Ansari, M.A. Barakat, A. Aljaafari, M.H. Cho. A polyaniline@MoS2-based organic–inorganic nanohybrid for the removal of Congo red: adsorption kinetic, thermodynamic and isotherm studies. New Journal of Chemistry. 42 (2018) 18802-18809.

[37] S. Singh, S. Perween, A. Ranjan, Dramatic enhancement in adsorption of Congo red dye in polymer-nanoparticle composite of polyaniline-zinc titanate. Journal of Environmental Chemical Engineering.9 (2021) 105149.

[38] L. Wang, A. Wang. Adsorption characteristics of Congo red onto the chitosan/montmorillonite nanocomposite.Journal of Hazardous Materials. 147 (2007) 979-985.

[39] V.K. Gupta, D. Pathania, N.C. Kothiyal, G. Sharma. Polyaniline zirconium (IV) silicophosphate nanocomposite for remediation of methylene blue dye from waste water. Journal of Molecular Liquids .190 (2014) 139-145.

[40] M. Maruthapandi, V.B. Kumar, J.H.T. Luong, A. Gedanken. Kinetics, isotherm, and thermodynamic studies of methylene blue adsorption on polyaniline and polypyrrole macro-nanoparticles synthesized by C-dot-initiated polymerization. ACS Omega. 3 (2018) 7196-7203.

[41] S. Agarwal, I. Tyagi, V.K. Gupta, F. Golbaz, A.N. Golikand, O. Moradi. Synthesis and characteristics of polyaniline/zirconium oxide conductive nanocomposite for dye adsorption application.Journal of Molecular Liquids. 218 (2016) 494-498.

[42] M.M. Ayad, A. Abu El-Nasr, J. Stejskal. Kinetics and isotherm studies of methylene blue adsorption onto polyaniline nanotubes base/silica composite.Journal of Industrial and Engineering Chemistry. 18 (2012) 1964-1969.

[43] R. Pandimurugan, S. Thambidurai. Synthesis of seaweed-ZnO-PANI hybrid composite for adsorption of methylene blue dye.Journal of Environmental Chemical Engineering. 4 (2016) 1332-1347.

[44] M.M. Ayad, A. Abu El-Nasr. Adsorption of cationic dye (Methylene Blue) from water using polyaniline nanotubes base. Journal of Physical Chemistry C. 114 (2010) 14377-14383.

[45] Z.H. Mahmoud, R.A. AL-Bayati, A.A. Khadom. Synthesis and supercapacitor performance of polyaniline-titanium dioxide-samarium oxide (PANI/TiO_2-Sm_2O_3) nanocomposite.Chemical Papers. 76 (2022) 1401-1412.

[46] X. Geng, R. Yi, X. Lin, C. Liu, Y. Sun, Y. Zhao, Y. Li, I. Mitrovic, R. Liu, L. Yang, C. Zhao. A high conductive TiC–TiO2/SWCNT/S composite with effective polysulfides adsorption for high performance Li–S batteries.Journal of Alloys and Compounds.851 (2021) 156793.

[47] S.U. Rahman, P. Röse, A.U.H.A. Shah, U. Krewer, S. Bilal, S. Farooq. Exploring the Functional Properties of Sodium Phytate Doped Polyaniline Nanofibers Modified FTO Electrodes for High-Performance Binder Free Symmetric Supercapacitors. Polymers.13 (2021) 2329.

[48] R. Pal, S.L. Goyal, I. Rawal, A.K. Gupta, Ruchi. Efficient energy storage performance of electrochemical supercapacitors based on polyaniline/graphene nanocomposite electrodes. Journal of Physics and Chemistry of Solids.154 (2021) 110057.

Scheme 1

Scheme 1 is available in Supplementary Files section.

Figures

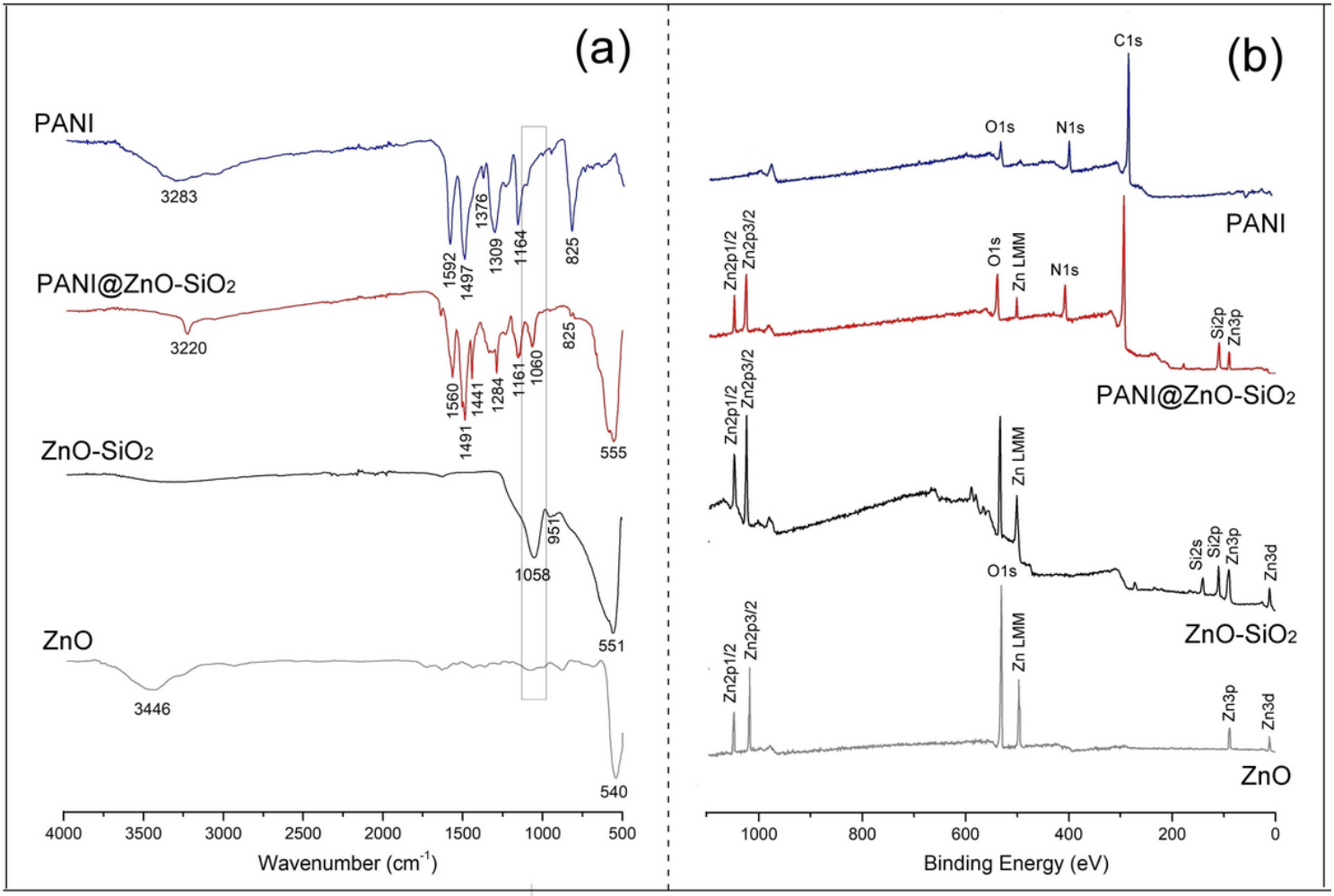

Figure 1

(a): FTIR analysis and (b): Survey XPS spectra of samples

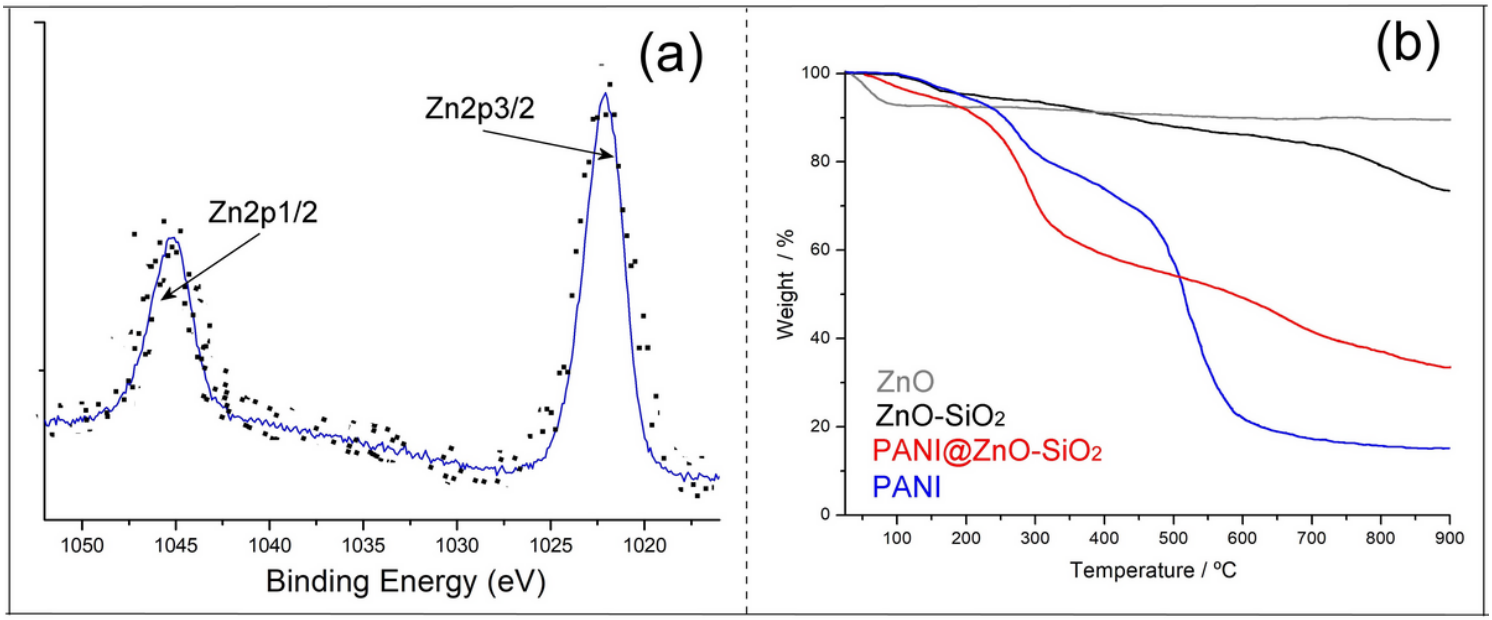

Figure 2

(a): XPS spectra for Zn2p signals of ZnO and (b):TGA curves of samples

Figure 3

XPS spectral: (a) Si2p signals of ZnO–SiO_2, (b) O1s of ZnO–SiO_2, (c) N1s of PANI and (d) N1s of PANI@ZnO–SiO_2.

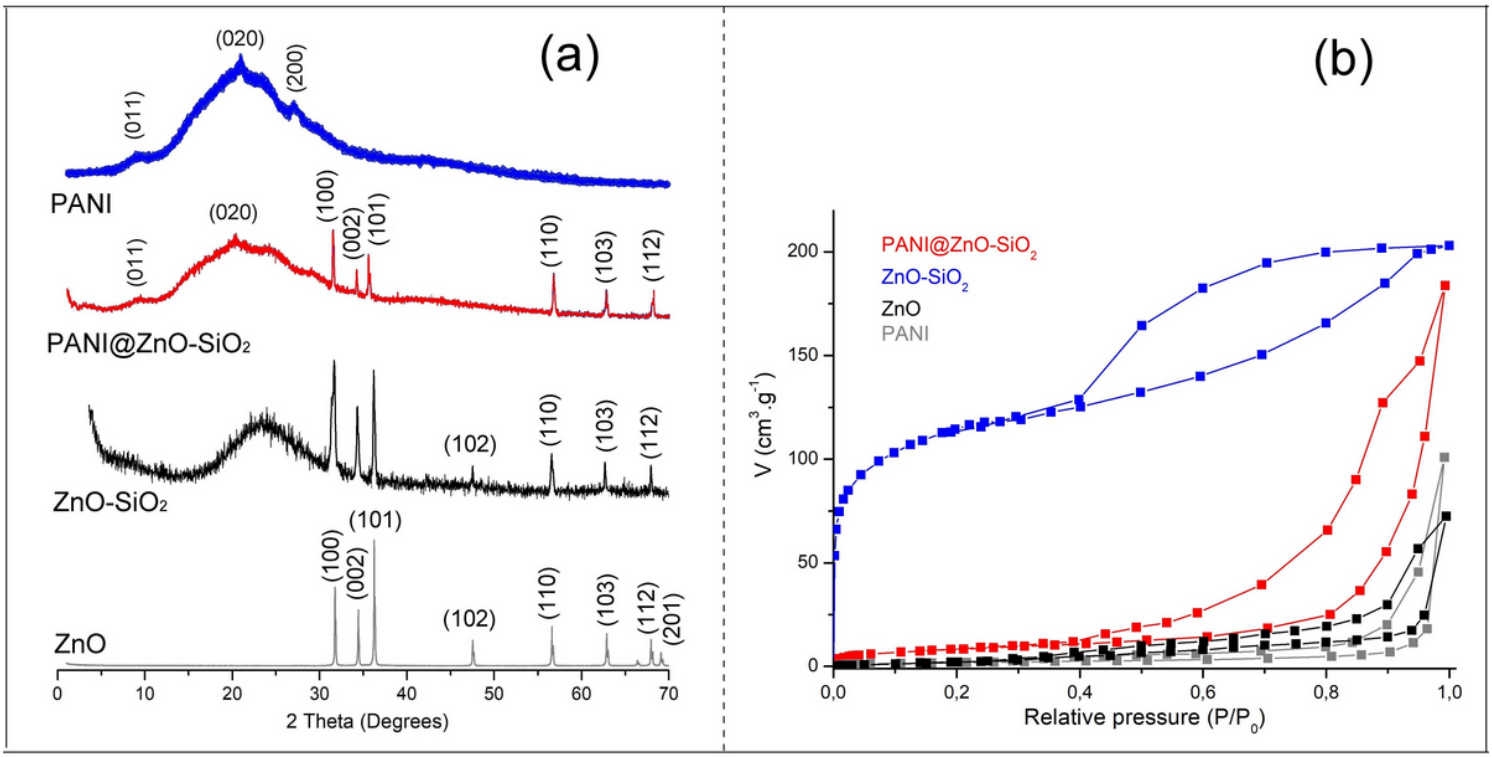

Figure 4

(a): XRD patterns and (b): (a) BET surface area of samples.

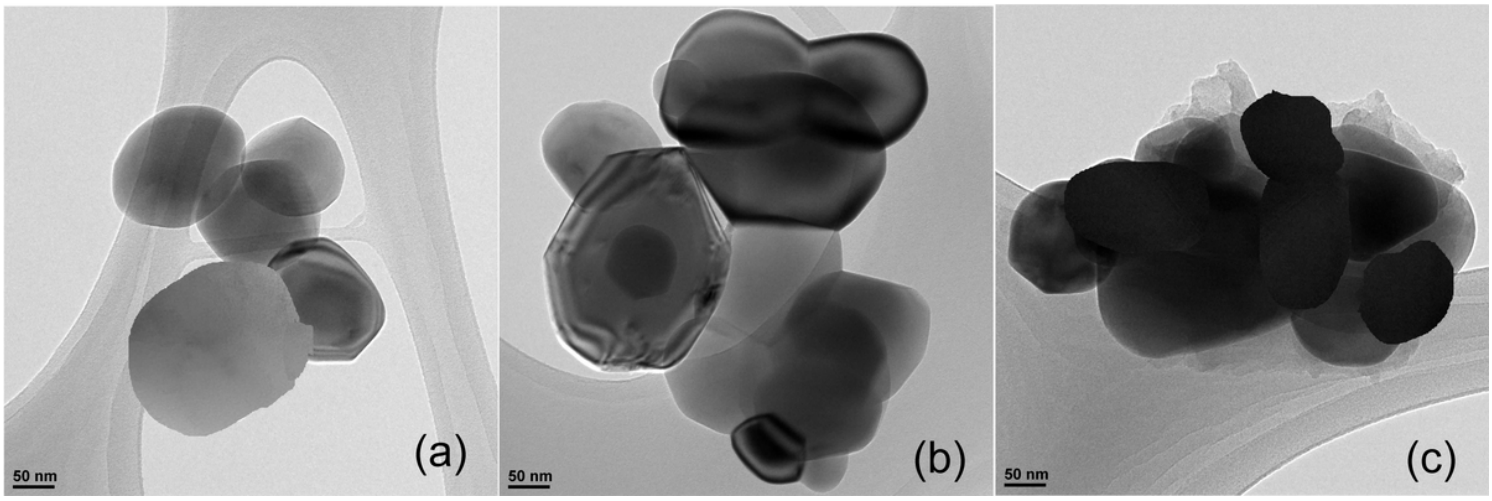

Figure 5

TEM images of : (a) ZnO, (b) ZnO–$SiO_2$and (c) PANI@ZnO–SiO_2.

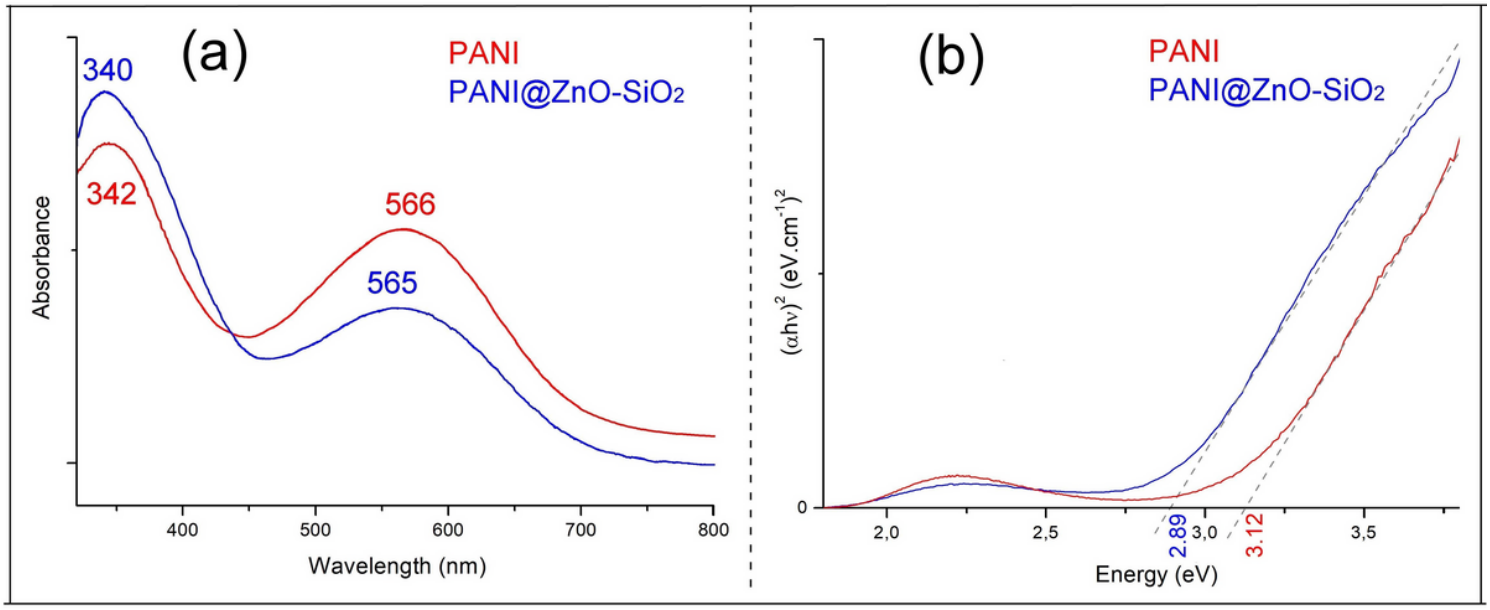

Figure 6

(a): UV-visspectroscopy absorption spectra and (c): Tauc plots of samples.

Figure 7

(a):Adsorption capacity (adsorbent dose: 100mg; V_{Dye}: 100mL; C_0: 100 $mg.L^{-1}$; T: 298K; pH 7.0; t = 4h) and (b): Cyclic voltammograms response of samples.

Figure 8

(a): Galvanostatic charge/discharge (GCD) response, (b): The galvanostatic cycling curve of materials electrode (1500 GCD cycles), the inset of (b): the galvanostatic cycling data collected at 1.5 $A.g^{-1}$.

Supplementary Files

This is a list of supplementary files associated with this preprint. Click to download.

- Sheme.png